# Post-LGM glacial retreat and Early Holocene monsoon intensification drives aggradation in the interiors of the Kashmir Himalaya

Saptarshi Dey[1], Naveen Chauhan[2], Pritha Chakravarti[1], Anushka Vasishtha[1], and Vikrant Jain[1]

1 – Earth Science Discipline, Indian Institute of Technology Gandhinagar, Palaj- 382355, Gujarat, India.

2 – Atomic Molecular and Optical Physics Division, Physical Research Laboratory Ahmedabad- 380009, Gujarat, India.

Corresponding author email –

saptarshi.dey@iitgn.ac.in

Co-author email list-

chauhan@prl.res.in

pritha.c@iitgn.ac.in

anushka.vashistha@alumni.iitgn.ac.in

vjain@iitgn.ac.in

This paper is a non-peer reviewed preprint submitted to EarthArXiv and currently in review in ***Quaternary Research*** (Cambridge core journal). DOI of the accepted manuscript will be attached here.

## Abstract

Understanding the response of glaciated catchments to climate change is crucial for assessing sediment transport from the high-elevation, semi-arid sectors in the Himalaya. The fluvioglacial sediments stored in the semi-arid Padder valley in the Kashmir Himalaya record valley aggradation during ~20 -10 ka. We relate the initial stage of valley aggradation to increased sediment supply from the deglaciated catchment during the glacial-to-interglacial phase transition. Previously-published bedrock-exposure ages in the upper Chenab River valley suggest ~180 km retreat of the valley glacier during ~20 - 15 ka. Increasing roundness of sand-grains and reducing mean grain-size from the bottom to the top of the valley-fill sequence hint about increasing fluvial transport with time and corroborate with the glacial retreat history. The later stages of aggradation can be attributed to strong monsoon during the early Holocene. Especially, the hillslope debris that drapes the fluvioglacial sediment archive may have resulted from the early Holocene monsoon maximum. We observe a net degradation of the valley-fill in the Holocene reflecting the weakening of summer monsoon or reduced input from the glaciers. Our study highlights the coupled effect of deglaciation and monsoon intensification in sediment transfer from the high-elevation sectors of the Himalaya.

## Keywords

Aggradation; deglaciation; Last Glacial Maximum; Indian Summer Monsoon; luminescence dating; Kashmir Himalaya.

## 1. Introduction

Understanding the role of past climate change on surface processes is essential to forecast how landscapes could respond to global warming. For example, changes in temperature and precipitation can have a strong impact on weathering (Dosseto et al., 2015), surface runoff, and sediment transport from the mountain to the basin (e.g., Tucker and Slingerland, 1997; Bookhagen et al., 2005; Scherler et al., 2015). The global warming poses greater implications for high-mountain areas as it would trigger extensive deglaciation and glacial retreat (e.g., Benn and Owen, 2002; Barnard et al., 2006; Eugster et al., 2016; Rashid et al., 2017). As a glacier retreats, it releases massive volumes of sediments in the drainage system as glacial outwash (e.g., Meigs et al., 2006; Smith et al., 2017). The glacial outwash is further transported downstream by fluvial systems.

Sediment transport from the Himalaya to the foreland basin over millennial timescales is suggested to be driven by climatic fluctuations such as glacial-interglacial phase transitions (e.g., Joussain et al., 2016) and intensified monsoon phases (e.g., Bookhagen et al., 2005; Dey et al., 2016). Present understanding of the climatic variations over $10^3$-$10^5$-years timescales suggests that the climatic cycles are dependent on Earth's orbital parameters, such as eccentricity and orbital precision (Milankovich, 1941). While the eccentricity cycles over ~100 ka cause the glacial-interglacial cycles, the ~21-23 ka precision is suggested to be driving the monsoonal variations (Milankovich, 1941). Foreland-bound sediments are often transiently-stored within the river valleys and intermontane basins across the entire Himalayan orogen. These sediment archives help us examine the role of climatic fluctuations behind spatiotemporal variability in sediment flux (e.g., Bookhagen et al., 2006; Scherler et al., 2015; Dey et al., 2016; Dutta et al., 2018). Over the last couple of decades, many of the major Himalayan drainages and intermontane valleys have been studied to obtain sedimentological and chronological constraints on the transiently-stored valley-fills. The studies spanned throughout the entire Himalayan front- from the eastern Himalaya (e.g., Srivastava et al., 2009; Panda et al., 2020), the central Himalaya (e.g., Pratt Sitaula et al., 2004; Meetei et al., 2007; Singh et al., 2017) and the western Himalaya (e.g., Bookhagen et al., 2006; Suresh et al., 2007;

Ray and Srivastava, 2010; Sinha et al., 2010; Dutta et al., 2012; Vassallo et al., 2015; Dey et al., 2016; Dutta et al., 2018). Interestingly, most studies have been conducted in humid to extreme-humid zones near the orographic front, where decoupling the glacial cycles and monsoon cycles are tricky. Continental oxygen isotope proxy (e.g., Cheng et al., 2016) and Northern Hemisphere Summer Solar Insolation (NHSI) data (Huybers, 2006) suggest that the glacial-interglacial cycle and monsoon cycles broadly overlap with each other. Therefore, understanding the impact of monsoon variability and glaciation-deglaciation by assessing intermontane valley archives is often challenging. To decouple the effect of deglaciation and monsoon intensification, we must investigate a well-preserved sediment archive in the semi-arid sectors of the Himalaya, which has glaciated catchments nearby and also attracts monsoon clouds. Typically, the semi-arid zones of the Himalaya are situated at high elevations (> 2 km above mean sea level) far from the mountain front (≥100 km) and the annual rainfall is lower than < 1 m/yr. A sharp rainfall gradient is maintained by the main orographic barrier formed by the Higher Himalaya (Bookhagen and Burbank, 2010) or the Lesser Himalayan duplex at places (e.g., Gavillot et al., 2018) (Supplementary Fig. S1). The orographic barrier is breached only during abnormal monsoon years or protracted strong monsoon (Bookhagen et al., 2005). The rain-shadow zones of the western Himalaya show significant glacial coverage at present and in the geological past (Owen et al., 2008) (Fig. 7a). In the last decade, scientists have explored climatic and tectonic implications of valley-fills in arid interiors of the Himalaya (e.g., Srivastava et al., 2013; Blöthe et al., 2014; Kumar and Srivastava, 2017; Chahal et al., 2019). Some of the studies favored the role of deglaciation in transient aggradation of river valleys (e.g., Ray and Srivastava, 2010; Sharma et al, 2016; Kothyari et al., 2017). Still, the data is sparse, and a concise understanding of sediment transfer from climatic transition zones is missing.

In pursuit of a better understanding of the role of late Pleistocene- early Holocene climate change in sediment transport in glaciated catchments, we investigated the sediment archive from the Padder valley in the Kashmir Himalaya (cf. Fig.1 for location). In this study, we combined detailed field observations on valley morphology, sedimentology, and sediment chronology to explore how sediment archives can record evidence of glacial retreat and monsoon intensification.

## 2. Geological background

The Padder valley is situated at the southeastern margin of the Kishtwar tectonic window in the Kashmir Himalaya interiors at an elevation of ~1750-1760m above mean sea-level (Fig. 1). The Kishtwar Window exposes the Lesser Himalayan duplex which is undergoing rapid exhumation at a rate of ~3 – 3.5 mm/yr since at least the last few million years and it forms the orographic barrier for the Indian Summer Monsoon (Gavillot et al., 2018; Dey et al., 2021) (Supplementary Fig. S1). In the upstream, however, the Higher Himalayan crystalline and medium-high grade Higher Himalayan metasediments are exposed, which exhume at a much slower rate (~0.2-0.4 mm/yr) (Gavillot et al., 2018). The valley is drained by the Chenab River, which originates in the Lahaul-Spiti region of northern Himachal Pradesh, India and traverses ~350 km till it reaches the Padder valley. The 'U-shaped' Padder valley (Fig. 2a) indicates glacial occupancy in the past. However, it is unknown at which time-period the glaciers came down to this valley. Previous works suggest that the upper Chenab valley has been subjected to glacial advancement and retreat (Kulkarni et al., 2007; Eugster et al., 2016). Eugster et al., (2016) constrained the advancement of the Chenab valley glacier by $^{10}$Be exposure ages from glacially-polished Higher Himalayan bedrock. In Fig.2, we portrayed the longitudinal elevation profile of the Chenab River and marked the temporal variations in glacial extent after Eugster et al., (2016). Around ~20 ka, the Chenab valley glacier was at ~2400m above msl (marked by point G1 in Fig. 7), while about ~15 ka ago, the glacier was at

~4150m above msl (point G4 in Fig. 7). Eugster et al., (2016) documents ~180 km glacial retreat towards upstream within a span of only 5-6 ka. There is no record of historical seismicity in the nearby regions in the upstream, neither this area has recorded any significant earthquake (Mw>3.5) in the last few decades (ISC catalogue; Supplementary Figure S2).

## 3. Methods

### 3.2. Luminescence chronology

Luminescence dating is a widely-accepted method for assessment of sediment depositional ages across various depositional environments, including fluvial (e.g., Fuchs and Lang, 2001; Cunningham and Wallinga, 2012), glacial (e.g., Hu et al., 2015; Mehta et al., 2012), Aeolian (e.g., Lai et al., 2009; Kumar et al., 2017) and lacustrine (e.g., Fan et al., 2010; Long et al., 2011) settings. To obtain the timing of deposition of sediments, we took five samples from the medium-fine sand layers (SD/P01-P05) exposed in the sediment archive much above the present-day channel and one sample from the fine sand layer from the lowermost terrace (SD/P06) for OSL measurement (Fig. 4a). The sand from the same layers was further used for grain-size and grain-shape analysis.

All samples were collected in galvanized iron pipes and opened only in subdued red light (wavelength ~650 nm) in the laboratory. The outer ~3 cm of each end of the pipes were discarded to avoid accidental exposure to sunlight during sample procurement. Quartz grains of 90-150 µm size fraction was extracted using standard separation protocol (Aitken, 1998) in Physical Research Laboratory, Ahmedabad. 24 aliquots of each sample were measured using Risoe TL-OSL reader in Physical Research Laboratory, Ahmedabad. The Equivalent dose (De) for each sample was measured using the OSL Double SAR (Single Aliquot Regenerative) protocol (Roberts, 2007). The Double-SAR protocol was used to surpass the luminescence signal from tiny feldspar inclusions within individual quartz grains (Fig. 5a). The aliquots were preheated to 240°C for 60 seconds. The instrument is equipped with blue light emitting diodes (LEDs) ($\lambda$=458 ± 10 nm). A UV filter (Hoya U-340) was used along with a solid-state photo-multiplier tube (PMT). Beta irradiation was made using a $^{90}Sr$ / $^{90}Y$ source. The three mandatory test doses for all the samples were set in the range of 25 - 120 Gy. For example, the test doses for sample SD/P02 were set for 37.5 Gy, 75 Gy and 112.5 Gy (Fig. 5b). The aliquots were considered for ED estimation only if: (i) recycling ratio was within 1±0.1, (ii) ED error was less than 20%, (iii) test dose error was less than 10%, and (iv) recuperation was below 5% of the natural. As all the samples show over-dispersion value < 20%, we used Central Age Model (CAM) to estimate Equivalent Dose (De) (Bailey and Arnold, 2006). Mean De ± 1σ for the samples are reported in Table 1.

Thick source ZnS (Ag) alpha counter was used for determining the elemental concentrations of Uranium and Thorium, while the Potassium ($^{40}K$) concentrations were estimated using NaI (Tl) gamma ray spectrometry. The dose rate was estimated using online software DRAC (Durcan et al., 2015) from the concentrations of Uranium (U), Thorium (Th), and Potassium (Table 1). The estimation of moisture content was done using the fractional difference of saturated vs. unsaturated sample weight (Table 1).

## 3.3. Sediment analysis

We sampled the same sand layers which were used for OSL dating. Samples were dried in a hot-air oven at 50˚C. And then, ~2 kg of each sample was used for sedimentological analysis.

### *3.3.1. Sediment grain-size analysis*

Each sample was dry-sieved using 1000 µm, 750 µm, 300 µm, 250 µm, 125 µm and 50 µm test sieves. Sediments above 1000 µm (very coarse-gravelly sand) and below 50 µm (silt) were discarded for grain-size analysis. In figure 6d, the sediment grain-size distribution (by weight %) for the samples are plotted against φ values, which represent the mean size of the mesh. A higher φ value indicates a smaller grain-size. The choice of mesh follows the convention of >1000 µm (granular sand, φ ~-2 to -1), 750-1000 µm (very coarse-grained, φ~-1-0), 300-750 µm (coarse-grained, φ=0-1), 150-300 µm (medium-grained, φ=1-2), 90-150 µm (fine-grained, φ=2-3) and 50-90 µm (very fine-grained, φ=3-4).

#### *3.3.2. Grain roundness*

We performed the coning and quartering method several times with the initial mass to finalize 100g of each sample for sediment shape analysis. We separated the quartz grains from the mix by Frantz isodynamic magnetic separator and used quartz as the index grain. The reason behind choosing quartz is that they are the most abundant and robust mineral in the mix. Grain-shape was calculated using Powers roundness index (Powers, 1953), where roundness is given by the formula-

$$Roundness = r/R \qquad \text{(Equation 1)}$$

Here, $r$ = mean radius of the inscribed circles at the edges of the grain and R = radius of the largest inscribed circle within the grain. We made 20 discs of each sample and measured the r and R of at least 20 grains per disc using a scaled Leica microscope (Fig. 6c). So, the minimum number of counts per sample is 120. The higher the roundness index, the more rounded the grains are. Grain-shape analysis results are plotted against mean grain-size in Fig. 6e. Results of the sedimentological analysis are listed in Supplementary Table S1.

## 4. Results

### 3.1. Field observation

The Padder valley records ~100m thick aggraded sediment sequence (Fig. 3b, 4a). The valley-fills are comprised of angular boulders, sub-rounded to rounded pebbles, sand of different grain-sizes, and occasional silt layers (Fig.4). The boulders and pebbles are mostly of Higher Himalayan origin, as it represents rocks of Higher Himalayan gneisses and high-grade schists. The whole sediment archive (Fig. 3a) can be split into several pulses of sediment flux. Each of these sediment package exhibits a fining-upward sequence. The lowermost units are usually boulders and pebbles, followed by gravel beds and ultimately fine sand to silt horizons (Fig. 2b). In the lower part of the sediment log, the clast size of the coarser fraction is higher and the clasts are more angular (Fig. 2b, 4c and 4d). However, near the top of the log, the clasts are smaller (mostly pebbles and occasional small boulders) and the clasts are more rounded (Fig. 2c and 4d). The change in grain-size from the bottom to the top of the archive is also seen in sand fractions. The change in size and roundness of the sand grains in sample SD/P-05 and SD/P-02 is visible in Fig. 6a and 6b. The valley-fills are punctuated by a series of coarse-grained and clast-supported angular debris units. The clast composition is dominantly quartzites and leucogranites (Fig. 2d, 2e).

The valley-fill sediments are re-incised by the Chenab River, and that has sculpted at least five terrace levels in the valley (Fig. 3a, 3b). Terraces (T1-T5) are classified according to their decreasing heights from the river (Fig. 3a). The river is still incising the valley-fill in the study area. The terrace T5 lying close to the river has a ~3 – 4 m thick cover of very well-sorted, well-rounded fine sand. The sand layer lacks proper lamination.

### 4.2. OSL chronology

Sample SD/P-01 and SD/P-02, taken from the base of the valley-fill, show depositional ages of 18.8±0.9 ka and 17.2±0.9 ka, respectively (Table 1). Samples SD/P-03 and SD/P-04, taken from the middle of the valley-fill, portrays depositional ages of 15.9±1.6 ka and 14.3±1.7

ka, respectively. Sample SD/P-05 taken near the top of the valley-fill (beneath the hillslope colluvium) provides an age of 11.3±1.3 ka. Sample SD/P-06 from the fine sand layer exposed in terrace T5, near the riverbed, returns a depositional age of 2.6±0.2 ka.

### 4.3. Sediment analysis

The samples collected from the valley-fill stored in the study area show large variations in the shape and size of the sand grains from the bottom to the top of the sediment log (Fig. 6d). Samples SD/P-01 and SD/P-02, collected from the bottom of the log show a high mean grain-size (φ ~0-1); whereas, samples SD/P-03 and SD/P-04, taken from the middle of the log, yield a lower mean grain-size (φ~2-3) and samples SD/P-05 and SD/P-06 yield even smaller mean grain-size (φ~3) (Fig.6d). The roundness coefficient (according to equation 1, described in section 3.3.2) varies from 0.27±0.08 to 0.60±0.07 (Fig. 6e). Among late Pleistocene samples, sample SD/P-01 has the lowest roundness (0.27±0.08), and sample SD/P-05 has the highest roundness (0.60±0.07), while late Holocene sample SD/P06 has an approximately similar roundness value of 0.55±0.14.

## 5. Discussion

We compiled our field observation, chronological and sedimentological analysis of the aggraded sediments and compared our results with previously-published record of glacial dynamics in the upper Chenab valley to assess the potential role of deglaciation and monsoon intensity in sediment aggradation observed in the Padder valley.

### 5.1. Sediment architecture and aggradation history

The Padder valley records ~90-100m thick sedimentary valley-fill (Fig.3b, 4a). The valley-fill units vary in grain-size ranging from fine silt to boulders having diameter~ 1m (Fig.4b). We observe an overall decrease in the clasts' size in conglomeratic layers from the bottom to the top of the archive (Fig. 4a). The lower and the middle part of the litholog are dominated by angular, poorly-sorted boulders, pebbles and gravels (Fig.4b, 4c). These layers contain clasts from Higher Himalayan crystallines and high-grade metasediments. Therefore, it is assumed that the sediment flux is not originating from the neighboring valley walls, as it would show Lesser Himalayan composition (leucogranites and quartzites) (cf. lithological map, supplementary Fig. S3). The whole sediment package can be subdivided into at least 5 sub-stages. Each sub-sections exhibit a fining-upward sequence (Fig. 4). The sub-sections contain angular-to-subangular boulders/ pebbles at the bottom, followed by a layer of gravel and topped by fine sand -silt layer. The sand layers are relatively less prominent (Fig.4a). These sediments are horizontally-layered. We identify these packages as typical glacial outwash deposits (e.g., Maizels, 2002). Although, the sand layers are relatively less prominent in the archive, we found several isolated 1-1.5m thick sand layers in all those sedimentary sub-sections and were able to constrain the depositional ages by OSL dating. The lower part of the valley-fills shows depositional age of ~16 - 20 ka (age of samples- SD/P-01: 18.8±0.9 ka and SD/P-02: 17.2±0.9 ka) (Fig.4a, Table 1). In the middle of the litholog, the depositional age is ~13-17 ka (age of samples- SD/P-03: 15.9±1.6 ka and SD/P-04: 14.3±1.7 ka). The topmost sample SD/P-05 taken from a ~1m thick sand layer between two well-polished and well-rounded pebble-boulder conglomerate layers yield depositional age of ~11.3±1.3 ka (Fig.4d). We identify these rounded clast-supported conglomerates as fluvial deposits. Notably, the upper part of the sediment archive contains ~20 - 25% clasts from the Lesser Himalayan terrain. The sediment sequence is topped by angular, poorly-sorted debris originated from the steep valley walls of the surrounding Lesser Himalayan units. Unfortunately, we could not find any dateable sand layer in the hillslope debris. In short, the Padder valley records net sediment aggradation by fluvioglacial during ~20 - 10 ka period and has been succeeded by hillslope debris flow. The absence of paleo-soil in between the fluvioglacial deposits and the hillslope debris suggests that the time-gap between the two phases of sedimentation could be very minimal (Fig. 4d).

The transiently-stored sediments are re-incised since then. The episodic re-incision is recorded by the formation of fluvial fill terraces along the Chenab River. The lowest terrace T5 records a ~4m thick fine sand capping (Fig. 2f). The sand capping is devoid of any recognizable laminations, the grain-size is lower and the sorting is higher than fluvioglacial sand samples (Fig.6a). The equivalent dose estimates from sample SD/P-06 are also clustered, having low over-dispersion value (OD ~ 6%, cf. Table 1), suggesting a uniformly well-bleached sample. We interpret the sand layer as an aeolian deposit. This kind of aeolian deposit is common in the arid western Himalaya (e.g. Kumar et al., 2017). A single depositional age from this aeolian sand layer suggests late Holocene age (age-SD/P-06: 2.6±0.2 ka).

### 5.2. Inconclusive role of tectonic forcing or landslides behind formation of the sediment archive

Gavillot et al., (2018) published a long-term exhumation history of the entire southeastern Kashmir Himalaya spanning across the Chenab watershed. It proposes that the western margin and the core of the Kishtwar Window is exhuming at a faster rate (3.2 – 3.6 mm/yr) than the surroundings (0.3 – 0.8 mm/yr) at least since Quaternary (Supplementary Fig. S2). In our recent study (Dey et al., 2021), we confirmed that these rates are persistent even over late Pleistocene timescale. However, none of these two aforementioned studies could find any ongoing faulting in the eastern margin of the KW and even in the upstream segment of the Chenab valley. Seismic epicenter maps of this region (Supplementary Fig. S3) show that there is a limited number of small to moderate magnitude earthquakes (Mw: 3 - 4) near Padder area and the seismicity is clustered near the western edge of the KW. The sediment sequence stored in the valley doesn’t record any penecontemporaneous deformation structures, defying the occurrence of seismic events during the deposition of sediments or shortly thereafter. Penecontemporaneous deformation structures in soft sediments are common features in Himalayan sediment archives impacted by concurrent seismicity (e.g., Kotlia and Rawat, 2004; Phartiyal and Sharma, 2009; Mugnier et al., 2011; Anoop et al., 2011). The Padder valley sediments contain enough sand and silt-clay that it could have recorded seismites, if there was any big seismic event at the time of formation of the archive. Apart from that, if we assume that the seismic activity was still ongoing, it should have triggered recurrent landslides. Large-scale seismic activity in the Himalaya could be responsible for the formation of landslide-dammed lakes (e.g., Korup et al., 2010; Kumar et al.,2021). These type of landslide-damming of the river creates lakes on the upstream side. However, in the Padder valley there is no lacustrine deposit at the base, rather the base contains the coarsest fraction. We have observed several landslides/ hillslope failures in the eastern fringes of the KW, but they are much smaller in size and probably incapable of blocking the Chenab River. Therefore, seismic trigger behind the sediment aggradation is inconclusive and mostly improbable.

### 5.3. Role of climate change in valley aggradation

#### *5.3.1. Global climate records*

Oxygen isotope proxy from terrestrial speleothems have been regarded as an indicator of tele-connected changes in atmospheric circulation and global climate. Oxygen isotope records denote fluctuations in monsoon intensity. More negative isotope ratios are linked to stronger atmospheric circulation and rainfall. High resolution ð$^{18}$O records from terrestrial cave speleothems recorded across the Indian subcontinent and Tibetan Plateau (e.g., Cheng et al., 2016; Dykoski et al., 2005; Wang et al., 2008; Dutt et al., 2015), from sea water in Andaman Sea (Marzin et al., 2013), from mineral composition from Arabian Sea sediment core (Deplazes et al., 2014), – all show high correlation for $10^2$ – $10^5$ -year timescale climatic fluctuations and therefore, can be regarded as indicators of global climate. We compare our data (Fig. 7d) with the ð$^{18}$O records from SanBao cave in eastern China (Cheng et al., 2016) (Fig. 7a), Northern Hemisphere summer (August) solar insolation data at 30˚N (Huybers, 2006) (Fig. 7b) and global sea-level change curve (Lambeck et al., 2014) (Fig. 7c). Lowering of global sea-level has been attributed to phases of extensive glaciation (e.g., Lambeck et al., 2002; Camoin et al., 2004). On the other hand, post-LGM (Last Glacial Maximum) sea-level rise caused by deglaciation and resulting meltwater pulses have been recorded worldwide (e.g., Lambeck and Chappel, 2001; Peltier, 2002; Harrison et al., 2019). Variations in the summer solar insolation pattern also define the glacial-interglacial phases (e.g., Gao et al., 2012).

#### *5.3.2. Post-LGM deglaciation in upper Chenab valley*

Now looking at the type of sediments and the depositional ages from the lower part of the archive, we can conclude that the sediments till at least 14 ka has been derived from the Higher Himalayan domain. Grain-size distribution and grain shape analysis of sampled sand layers from the aggraded sediment sequence show a systematic change in sediment characteristics with time. Grain-size analysis portrays an overall fining-upward sequence as the sub-sections (discussed in section 5.1) show a gradual decrease in grainsize across all size fractions- boulders to sand (Fig. 6d). The average roundness of the grains also increases from the bottom to the top (Fig. 6e). Fig. 6e illustrates a linear correlation between mean population grain-size and mean roundness co-efficient measured from the sand grains. It highlights that with time, the grain-size and angularity of sand grains have reduced simultaneously. This can be related to increasing fluvial transport with time and could potentially point to a retreating glacier in the upstream. As the depositional attributes clearly point out a glacial source of sediments, we compared our results with the proposed history of deglaciation in Upper Chenab valley. Eugster et al., (2016) estimated the glacial extent along the upper Chenab valley with surface-exposure dating of glacially-polished bedrocks using $^{10}$Be. That study argued that ~20 ka, the valley glaciers advanced at least until ~2450 m above msl and resided only ~90 km upstream from the Padder valley (see point G1 in Fig. 8a, 8b). Whereas, in the next ~5 kyr, the valley glacier retreated ~180 km and was at point G4 (~4150 m above msl) (Fig. 8a, 8b). Similar glacial retreat must have been observed in the northern tributaries originating from the arid Zanskar Range. Now comparing the aggradation of the lower and middle units with the glacial retreat history, we find that those are synchronous. The absence of Lesser Himalayan granites and quartzites in the lower- middle half of the section confirms that local sediment source is negligible and sediments have come from upstream. With grain-size fining and increasing roundness with time, we relate the majority of the sediment aggradation to deglaciation in the upper Chenab valley or southern flank of the Zanskar Range, lying north of the Padder valley.

#### *5.3.3. Early Holocene monsoon intensification*

The grain-size distribution of the upper part of the sediment archive is nearly similar to the middle part of the section (Fig. 4a and 6d), but the grains/ clasts are much rounded in the upper section (Fig. 4d and 6e). Moreover, the upper section has ~20 – 25% of local sediment sources (i.e., lesser Himalayan leucogranites, quartzites, low-grade schists and mylonites from the nearby MCT shear zone). This is a hint that local hillslope processes were significant as well as transport of fluvioglacial sediments from the upstream. The roundness of the sand grains/ clasts (Higher Himalayan source) and clast-supported nature of deposits (Fig. 6d) ensure that there has been sufficient discharge and long transport. So, we consider that as fluvial deposit. Chronologically, the fluvial sediments deposited during ~13 – 10 ka (Table 1; Fig. 4a). Comparing the data with ð$^{18}$O records (Fig. 7a), we see that post the Younger Draya (YD) event at ~12.8 ka, the strength of Indian Summer Monsoon was monotonously increasing in early Holocene and was higher than the present-day monsoon standard. It reached a maximum at ~9 – 8 ka. We propose that the hillslope processes in the Padder area accentuated in this time-window of strong monsoon. The hillslope debris that accumulated sometime after 11 ka, may well represent the strong monsoon phase ~11 – 9 ka (e.g., Cheng et al., 2016; Dutt et al., 2015). The hillslope debris cones are ubiquitous and hint a wetter climate. There is no record of past seismicity that could trigger such widespread landslide or hillslope failure.

The present-day rainfall amount in the Padder valley or upstream is ≤ 1 m/yr (Bookhagen and Burbank, 2006). It is shielded from the monsoon clouds by the rapidly-exhuming Kishtwar tectonic window (Gavillot et al., 2018; Dey et al., 2021). However, if we assume that the upper part of the sediment archive formed during strong monsoon ~14 – 9 ka (Cheng et al., 2016) (Fig. 7a), the monsoon clouds must have penetrated the orographic barrier imparted by the Kishtwar Window. At this moment, we do not have proper constraints on such temporal variations in rainfall distribution.

### *5.3.4. Holocene terrace formation and late Holocene aridity*

The Padder valley records at least five levels of fill terraces which has been episodically sculpted into the fluvioglacial sediment archive. These re-incision phases marked by formation of each terrace levels can be correlated with monsoon weakening during Holocene. Similar Holocene terrace records are obtained from the Sutlej valley (Bookhagen et al., 2006) and the Kangra Valley (Dey et al., 2016). The presence of aeolian deposits in late Holocene reflects increasing aridity in the study area (sample SD/P-06: 2.6±0.2 ka). We have very limited age control on the aeolian deposition. Based on OSL-dated moraines, Bisht et al. (2019) proposed a protracted arid phase during ~5 – 3 ka in the western Himalaya. Another study by Khan et al. (2018) claims a period of aridity during 4 – 1 ka in the Himalaya. The loess deposit in Padder valley could be broadly linked with this dry phase. In addition to this, CIA (Chemical index of alteration) records from Kutch region in western India depict a dry phase during 4.2 – 2.5 ka (Ngangom et al., 2017) and corroborates well with the onset of the debated ‘Meghalayan age’ ~4.2 ka (Shankar, 2021). The Meghalayan age starts with a drought, therefore, overall increase in aridity is expected.

#### *5.3.5. A short summary and caveats*

We observe that the timing of initial and middle stages of sediment aggradation in the Padder valley correlates well with the timing of the transition from the glacial (LGM) to the interglacial phase. The globally-accepted duration of the LGM is ~26-19 ka (Clark et al., 2009). Although there exist some chronological ambiguities for post-LGM deglaciation from the Himalaya, by assessing the process and analytical uncertainties of our dating method and previously-published chronological constraints on glacial fluctuations in upper Chenab valley (Eugster et al., 2016), we propose that the majority of sediment aggradation resulted from post-LGM deglaciation caused by global as well as a regional temperature change. We acknowledge that the post-LGM deglaciation is followed by late Pleistocene- early Holocene increased monsoon intensity (e.g., Gebregiorgis et al., 2016; Cheng et al., 2016) during ~15 – 9 ka (Fig. 7a). But majority of the sediment deposit was already there in the Padder valley before the onset of strong monsoon, therefore, those deposits (~70m thick as in Fig. 4a) are probably not linked to increase in monsoon strength. Therefore, we favor a dominant control of deglaciation behind formation of the Padder valley sediment archive. The phase of deglaciation was followed by monsoon intensification facilitating the hillslope processes.

### 5.4. Regional significance of our study

Sediment aggradation and re-incision in a majority of the NW Himalayan valleys since the late Pleistocene have been attributed to fluctuations in climate forcing- for example, Sutlej valley (Bookhagen et al., 2005), Kangra valley (Dey et al., 2016); Zanskar valley (Chahal et al., 2019); Goriganga valley (Ali et al., 2013), Baspa valley (Dutta et al., 2018), Spiti valley (Srivastava et al., 2013), Ganga valley (Dutta et al., 2012), Bhagirathi valley (Barnard et al., 2004), Alakananda valley (Juyal et al., 2010; Ray and Srivastava, 2010), Garhwal region (Scherler et al., 2015), etc. Nearly all the studies have documented valley aggradation by ~ fluvial and/or fluvioglacial sediments. However, it is tricky to decouple the monsoon-influenced and deglaciation-influenced aggradation during the post-LGM to early Holocene period. It is understood that the drainage systems that lie in the foreland-ward side of the main orographic barrier have a greater influence of the Indian Summer Monsoon and therefore, the valley aggradation is attributed to transient increase in sediment supply from the hillslopes driven by enhancement of monsoon rainfall during 16 - 9 ka (e.g., Bookhagen et al., 2005; Dey et al., 2016). Studies by Barnard et al., (2004), Kumar and Srivastava (2017) and Dutta et al., (2018) further propose that Indian Summer Monsoon can play a key role in sediment aggradation even in glacier-dominated catchments lying in the arid hinterland-ward side of the orographic barrier. In our case, the albeit the uppermost 20m of the sediment archive, the sedimentation can largely be linked to deglaciation in the upstream section. Glacial outwash is further transported downstream by the glacial melt and snow-melt. Only the upper part of the sediment archive hint towards an increased hillslope sediment flux triggered by the strong monsoon in the early Holocene. To summarize, this study explores the role of deglaciation and monsoon intensification in sediment aggradation in an arid and glaciated catchment in the interiors of the Kashmir Himalaya. At the same time, it highlights how glacial retreat can be traced by examining an outwash sediment archive.

## 6. Conclusions

Combining our observations, analytical results and previously-published literature, we conclude that-

a. Sediment archive in the Padder valley is dominated by fluvially-transported glacial outwash sediments and hillslope debris. The aggradation by fluvioglacial sediments happened during 20 – 13 ka, followed by fluvial succession during 13 – 10 ka and hillslope failure post 10 ka.

b. Increasing roundness and decreasing grainsize of sand within the fluvioglacial deposit favors the role of post-LGM glacial retreat in the genesis of sediments in the arid to semi-arid interiors of the Himalaya.

c. The hillslope debris may have resulted from monsoon maxima in early Holocene. During early Holocene (13 – 9 ka), the ISM strength was at its' peak and moisture must have penetrated the orographic barrier formed by the Kishtwar Window.

**Acknowledgments**

S. Dey is supported by DST-INSPIRE faculty research grant by the Department of Science and Technology, India (grant #DST/INSPIRE/04/2017/003278). Authors acknowledge the help from C. Singh, S. Das and A. Das during the fieldwork.

**References**

Aitken, M.J., 1998. Introduction to optical dating: the dating of Quaternary sediments by the use of photon-stimulated luminescence. Clarendon Press.

Ali, S. N., Biswas, R. H., Shukla, A. D., & Juyal, N. (2013). Chronology and climatic implications of Late Quaternary glaciations in the Goriganga valley, central Himalaya, India. Quaternary Science Reviews, 73, 59-76.

Anoop, A., Prasad, S., Basavaiah, N., Brauer, A., Shahzad, F., & Deenadayalan, K. (2012). Tectonic versus climate influence on landscape evolution: a case study from the upper Spiti valley, NW Himalaya. *Geomorphology*, *145*, 32-44.

Bailey, R.M. and Arnold, L.J., 2006. Statistical modelling of single grain quartz De distributions and an assessment of procedures for estimating burial dose. *Quaternary Science Reviews*, *25*(19-20), pp.2475-2502.

Barnard, P. L., Owen, L. A., & Finkel, R. C. (2004). Style and timing of glacial and paraglacial sedimentation in a monsoon-influenced high Himalayan environment, the upper Bhagirathi Valley, Garhwal Himalaya. Sedimentary Geology, 165(3-4), 199-221.

Barnard, P. L., Owen, L. A., Finkel, R. C., & Asahi, K. (2006). Landscape response to deglaciation in a high relief, monsoon-influenced alpine environment, Langtang Himal, Nepal. Quaternary Science Reviews, 25(17-18), 2162-2176.

Blöthe, J. H., Munack, H., Korup, O., Fülling, A., Garzanti, E., Resentini, A., & Kubik, P. W. (2014). Late Quaternary valley infill and dissection in the Indus River, western Tibetan Plateau margin. Quaternary Science Reviews, 94, 102-119.

Bookhagen, B., & Burbank, D. W. (2006). Topography, relief, and TRMM-derived rainfall variations along the Himalaya. Geophysical Research Letters, 33(8).

Bookhagen, B., Fleitmann, D., Nishiizumi, K., Strecker, M. R., & Thiede, R. C. (2006). Holocene monsoonal dynamics and fluvial terrace formation in the northwest Himalaya, India. Geology, 34(7), 601-604.

Bookhagen, B., Thiede, R. C., & Strecker, M. R. (2005). Late Quaternary intensified monsoon phases control landscape evolution in the northwest Himalaya. Geology, 33(2), 149-152.

Bookhagen, B., Thiede, R. C., & Strecker, M. R. (2005). Abnormal monsoon years and their control on erosion and sediment flux in the high, arid northwest Himalaya. *Earth and Planetary Science Letters*, *231*(1-2), 131-146.

Camoin, G. F., Montaggioni, L. F., & Braithwaite, C. J. R. (2004). Late glacial to post glacial sea levels in the Western Indian Ocean. Marine Geology, 206(1-4), 119-146.

Chahal, P., Kumar, A., Sharma, C. P., Singhal, S., Sundriyal, Y. P., & Srivastava, P. (2019). Late Pleistocene history of aggradation and incision, provenance and channel connectivity of the Zanskar River, NW Himalaya. Global and Planetary Change, 178, 110-128.

Cheng, H., Spötl, C., Breitenbach, S.F., Sinha, A., Wassenburg, J.A., Jochum, K.P., Scholz, D., Li, X., Yi, L., Peng, Y. and Lv, Y., 2016. Climate variations of Central Asia on orbital to millennial timescales. *Scientific Reports*, *6*(1), pp.1-11.

Clark, P.U., Dyke, A.S., Shakun, J.D., Carlson, A.E., Clark, J., Wohlfarth, B., Mitrovica, J.X., Hostetler, S.W. and McCabe, A.M., 2009. The last glacial maximum. science, 325(5941), pp.710-714.

Cunningham, A. C., & Wallinga, J. (2012). Realizing the potential of fluvial archives using robust OSL chronologies. *Quaternary Geochronology*, *12*, 98-106.

Deplazes, G., Lückge, A., Stuut, J.B.W., Pätzold, J., Kuhlmann, H., Husson, D., Fant, M. and Haug, G.H., 2014. Weakening and strengthening of the Indian monsoon during Heinrich events and Dansgaard-Oeschger oscillations. *Paleoceanography*, *29*(2), pp.99-114.

Dey, S., Thiede, R.C., Schildgen, T.F., Wittmann, H., Bookhagen, B., Scherler, D., Jain, V. and Strecker, M.R., 2016. Climate-driven sediment aggradation and incision since the late Pleistocene in the NW Himalaya, India. Earth and Planetary Science Letters, 449, pp.321-331.

Dosseto, A., Vigier, N., Joannes-Boyau, R. C., Moffat, I., Singh, T., & Srivastava, P. (2015). Rapid response of silicate weathering rates to climate change in the Himalaya.

Durcan, J.A., King, G.E. and Duller, G.A., 2015. DRAC: Dose Rate and Age Calculator for trapped charge dating. *Quaternary Geochronology*, *28*, pp.54-61.

Dutt, S., Gupta, A. K., Clemens, S. C., Cheng, H., Singh, R. K., Kathayat, G., & Edwards, R. L. (2015). Abrupt changes in Indian summer monsoon strength during 33,800 to 5500 years BP. *Geophysical Research Letters*, *42*(13), 5526-5532.

Dutta, S., Mujtaba, S. A. I., Saini, H. S., Chunchekar, R., & Kumar, P. (2018). Geomorphic evolution of glacier-fed Baspa Valley, NW Himalaya: record of Late Quaternary climate change, monsoon dynamics and glacial fluctuations. Geological Society, London, Special Publications, 462(1), 51-72.

Dutta, S., Suresh, N., & Kumar, R. (2012). Climatically controlled Late Quaternary terrace staircase development in the fold-and-thrust belt of the Sub Himalaya. Palaeogeography, Palaeoclimatology, Palaeoecology, 356, 16-26.

Dykoski, C.A., Edwards, R.L., Cheng, H., Yuan, D., Cai, Y., Zhang, M., Lin, Y., Qing, J., An, Z. and Revenaugh, J., 2005. A high-resolution, absolute-dated Holocene and deglacial Asian monsoon record from Dongge Cave, China. *Earth and Planetary Science Letters*, *233*(1-2), pp.71-86.

Eugster, P., Scherler, D., Thiede, R. C., Codilean, A. T., & Strecker, M. R. (2016). Rapid Last Glacial Maximum deglaciation in the Indian Himalaya coeval with midlatitude glaciers: New insights from 10Be-dating of ice-polished bedrock surfaces in the Chandra Valley, NW Himalaya. Geophysical Research Letters, 43(4), 1589-1597.

Fan, Q., Lai, Z., Long, H., Sun, Y., & Liu, X. (2010). OSL chronology for lacustrine sediments recording high stands of Gahai Lake in Qaidam Basin, northeastern Qinghai–Tibetan Plateau. Quaternary Geochronology, 5(2-3), 223-227.

Fuchs, M., & Lang, A. (2001). OSL dating of coarse-grain fluvial quartz using single-aliquot protocols on sediments from NE Peloponnese, Greece. *Quaternary Science Reviews*, *20*(5-9), 783-787.

Gao, L., Nie, J., Clemens, S., Liu, W., Sun, J., Zech, R., & Huang, Y. (2012). The importance of solar insolation on the temperature variations for the past 110 ka on the Chinese Loess Plateau. Palaeogeography, Palaeoclimatology, Palaeoecology, 317, 128-133.

Gebregiorgis, D., Hathorne, E. C., Sijinkumar, A. V., Nath, B. N., Nürnberg, D., & Frank, M. (2016). South Asian summer monsoon variability during the last~ 54 kas inferred from surface water salinity and River runoff proxies. Quaternary Science Reviews, 138, 6-15.

Harrison, S., Smith, D. E., & Glasser, N. F. (2019). Late Quaternary meltwater pulses and sea level change. Journal of Quaternary Science, 34(1), 1-15.

Hu, G., Yi, C. L., Zhang, J. F., Liu, J. H., & Jiang, T. (2015). Luminescence dating of glacial deposits near the eastern Himalayan syntaxis using different grain-size fractions. Quaternary Science Reviews, 124, 124-144.

Huybers, P. (2006). Early Pleistocene glacial cycles and the integrated summer insolation forcing. Science, 313(5786), 508-511.

Joussain, R., Colin, C., Liu, Z., Meynadier, L., Fournier, L., Fauquembergue, K., Zaragosi, S., Schmidt, F., Rojas, V. and Bassinot, F., 2016. Climatic control of sediment transport from the Himalayas to the proximal NE Bengal Fan during the last glacial-interglacial cycle. Quaternary Science Reviews, 148, pp.1-16.

Juyal, N., Sundriyal, Y., Rana, N., Chaudhary, S., & Singhvi, A. K. (2010). Late Quaternary fluvial aggradation and incision in the monsoon-dominated Alaknanda valley, Central Himalaya, Uttrakhand, India. *Journal of Quaternary Science*, *25*(8), 1293-1304.

Korup, O., Montgomery, D. R., & Hewitt, K. (2010). Glacier and landslide feedbacks to topographic relief in the Himalayan syntaxes. *Proceedings of the National Academy of Sciences*, *107*(12), 5317-5322.

Kothyari, G. C., Shukla, A. D., & Juyal, N. (2017). Reconstruction of Late Quaternary climate and seismicity using fluvial landforms in Pindar River valley, Central Himalaya, Uttarakhand, India. Quaternary International, 443, 248-264.

Kotlia, B. S., & Rawat, K. S. (2004). Soft sediment deformation structures in the Garbyang palaeolake: evidence for the past shaking events in the Kumaun Tethys Himalaya. *CURRENT SCIENCE-BANGALORE-*, *87*, 377-379.

Kulkarni, A. V., Bahuguna, I. M., Rathore, B. P., Singh, S. K., Randhawa, S. S., Sood, R. K., & Dhar, S. (2007). Glacial retreat in Himalaya using Indian remote sensing satellite data. Current science, 69-74.

Kumar, V., Jamir, I., Gupta, V., & Bhasin, R. K. (2021). Inferring potential landslide damming using slope stability, geomorphic constraints, and run-out analysis: a case study from the NW Himalaya. *Earth Surface Dynamics*, *9*(2), 351-377.

Kumar, A., & Srivastava, P. (2017). The role of climate and tectonics in aggradation and incision of the Indus River in the Ladakh Himalaya during the late Quaternary. Quaternary Research, 87(3), 363.

Kumar, A., Srivastava, P., & Meena, N. K. (2017). Late Pleistocene aeolian activity in the cold desert of Ladakh: a record from sand ramps. Quaternary international, 443, 13-28.

Lai, Z., Kaiser, K., & Brückner, H. (2009). Luminescence-dated aeolian deposits of late Quaternary age in the southern Tibetan Plateau and their implications for landscape history. Quaternary Research, 72(3), 421-430.

Lambeck, K., & Chappell, J. (2001). Sea level change through the last glacial cycle. Science, 292(5517), 679-686.

Lambeck, K., Rouby, H., Purcell, A., Sun, Y., & Sambridge, M. (2014). Sea level and global ice volumes from the Last Glacial Maximum to the Holocene. Proceedings of the National Academy of Sciences, 111(43), 15296-15303.

Lambeck, K., Yokoyama, Y., & Purcell, T. (2002). Into and out of the Last Glacial Maximum: sea-level change during Oxygen Isotope Stages 3 and 2. Quaternary Science Reviews, 21(1-3), 343-360.

Long, H., Lai, Z., Wang, N., & Zhang, J. (2011). A combined luminescence and radiocarbon dating study of Holocene lacustrine sediments from arid northern China. Quaternary Geochronology, 6(1), 1-9.

Maizels, J. (2002). Sediments and landforms of modern proglacial terrestrial environments. In Modern and past glacial environments (pp. 279-316). Butterworth-Heinemann.

Marzin, C., Kallel, N., Kageyama, M., Duplessy, J. C., & Braconnot, P. (2013). Glacial fluctuations of the Indian monsoon and their relationship with North Atlantic climate: new data and modelling experiments. *Climate of the Past*, *9*(5), 2135-2151.

Meetei, L. I., Pattanayak, S. K., Bhaskar, A., Pandit, M. K., & Tandon, S. K. (2007). Climatic imprints in Quaternary valley fill deposits of the middle Teesta valley, Sikkim Himalaya. Quaternary International, 159(1), 32-46.

Mehta, M., Majeed, Z., Dobhal, D. P., & Srivastava, P. (2012). Geomorphological evidences of post-LGM glacial advancements in the Himalaya: a study from Chorabari Glacier, Garhwal Himalaya, India. Journal of earth system science, 121(1), 149-163.

Meigs, A., Krugh, W. C., Davis, K., & Bank, G. (2006). Ultra-rapid landscape response and sediment yield following glacier retreat, Icy Bay, southern Alaska. Geomorphology, 78(3-4), 207-221.

Milankovich, M. (1941). Canon of insolation and the Ice-Age problems. R. Serbian Acad. Spec. Publ, 132.

Mugnier, J. L., Huyghe, P., Gajurel, A. P., Upreti, B. N., & Jouanne, F. (2011). Seismites in the Kathmandu basin and seismic hazard in central Himalaya. *Tectonophysics*, *509*(1-2), 33-49.

Ngangom, M., Bhandari, S., Thakkar, M. G., Shukla, A. D., & Juyal, N. (2017). Mid-Holocene extreme hydrological events in the eastern Great Rann of Kachchh, western India. *Quaternary International*, *443*, 188-199.

Panda, S., Kumar, A., Das, S., Devrani, R., Rai, S., Prakash, K., & Srivastava, P. (2020). Chronology and sediment provenance of extreme floods of Siang River (Tsangpo-Brahmaputra River valley), northeast Himalaya. Earth Surface Processes and Landforms, 45(11), 2495-2511.

Peltier, W. R. (2002). On eustatic sea level history: Last Glacial Maximum to Holocene. Quaternary Science Reviews, 21(1-3), 377-396.

Phartiyal, B., & Sharma, A. (2009). Soft-sediment deformation structures in the Late Quaternary sediments of Ladakh: Evidence for multiple phases of seismic tremors in the North western Himalayan Region. *Journal of Asian Earth Sciences*, *34*(6), 761-770.

Powers, M.C., 1953, A new roundness scale for sedimentary particles: Journal of Sedimentary Petrology, 23:117-119.

Pratt-Sitaula, B., Burbank, D. W., Heimsath, A., & Ojha, T. (2004). Landscape disequilibrium on 1000–10,000 year scales Marsyandi River, Nepal, central Himalaya. Geomorphology, 58(1-4), 223-241.

Rashid, I., Romshoo, S. A., & Abdullah, T. (2017). The recent deglaciation of Kolahoi valley in Kashmir Himalaya, India in response to the changing climate. Journal of Asian Earth Sciences, 138, 38-50.

Ray, Y., & Srivastava, P. (2010). Widespread aggradation in the mountainous catchment of the Alaknanda–Ganga River System: timescales and implications to Hinterland–foreland relationships. Quaternary Science Reviews, 29(17-18), 2238-2260.

Scherler, D., Bookhagen, B., Wulf, H., Preusser, F., & Strecker, M. R. (2015). Increased late Pleistocene erosion rates during fluvial aggradation in the Garhwal Himalaya, northern India. Earth and Planetary Science Letters, 428, 255-266.

Shankar, U. (2021). Cave 'Krem Mawmluh'of Meghalaya plateau–The base of the 'Meghalayan Age'and '4.2 ka BP Event'in Holocene (Anthropocene). *International Journal of Ecology and Environmental Sciences*, *47*(1), 49-59.

Sharma, S., Chand, P., Bisht, P., Shukla, A. D., Bartarya, S. K., Sundriyal, Y. P., & Juyal, N. (2016). Factors responsible for driving the glaciation in the Sarchu Plain, eastern Zanskar Himalaya, during the late Quaternary. Journal of Quaternary Science, 31(5), 495-511.

Singh, A. K., Pattanaik, J. K., & Jaiswal, M. K. (2017). Late Quaternary evolution of Tista River terraces in Darjeeling-Sikkim-Tibet wedge: Implications to climate and tectonics. Quaternary International, 443, 132-142.

Sinha, S., Suresh, N., Kumar, R., Dutta, S., & Arora, B. R. (2010). Sedimentologic and geomorphic studies on the Quaternary alluvial fan and terrace deposits along the Ganga exit. Quaternary International, 227(2), 87-103.

Smith, J.A., Andersen, T.J., Shortt, M., Gaffney, A.M., Truffer, M., Stanton, T.P., Bindschadler, R., Dutrieux, P., Jenkins, A., Hillenbrand, C.D. and Ehrmann, W., 2017. Sub-ice-shelf sediments record history of twentieth-century retreat of Pine Island Glacier. Nature, 541(7635), pp.77-80.

Srivastava, P., Bhakuni, S. S., Luirei, K., & Misra, D. K. (2009). Morpho-sedimentary records at the Brahmaputra River exit, NE Himalaya: Climate–tectonic interplay during the Late Pleistocene–Holocene. Journal of Quaternary Science: Published for the Quaternary Research Association, 24(2), 175-188.

Srivastava, P., Ray, Y., Phartiyal, B., & Sharma, A. (2013). Late Pleistocene-Holocene morphosedimentary architecture, Spiti River, arid higher Himalaya. International Journal of Earth Sciences, 102(7), 1967-1984.

Suresh, N., Bagati, T. N., Kumar, R., & Thakur, V. C. (2007). Evolution of Quaternary alluvial fans and terraces in the intramontane Pinjaur Dun, Sub-Himalaya, NW India: interaction between tectonics and climate change. Sedimentology, 54(4), 809-833.

Tucker, G. E., & Slingerland, R. (1997). Drainage basin responses to climate change. Water Resources Research, 33(8), 2031-2047.

Wang, Y., Cheng, H., Edwards, R.L., Kong, X., Shao, X., Chen, S., Wu, J., Jiang, X., Wang, X. and An, Z., 2008. Millennial-and orbital-scale changes in the East Asian monsoon over the past 224,000 years. Nature, 451(7182), pp.1090-1093.

Figures and tables for the manuscript titled

# Post-LGM Glacial Retreat and Early Holocene Monsoon Intensification Drives Aggradation in the Interiors of the Kashmir Himalaya

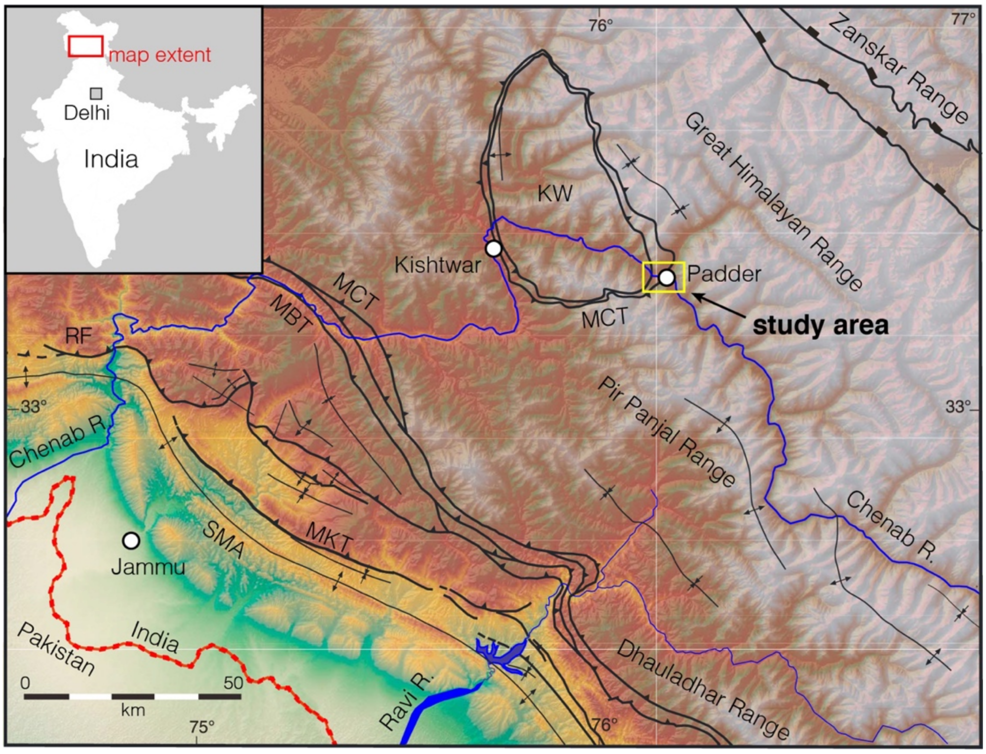


Figure 1: An overview map of the far-western Himalaya showing the Chenab drainage area (modified after Gavillot et al., 2018). Our study location (yellow rectangle) is near the town of Padder, at the southeastern margin of the Kishtwar Window (KW).

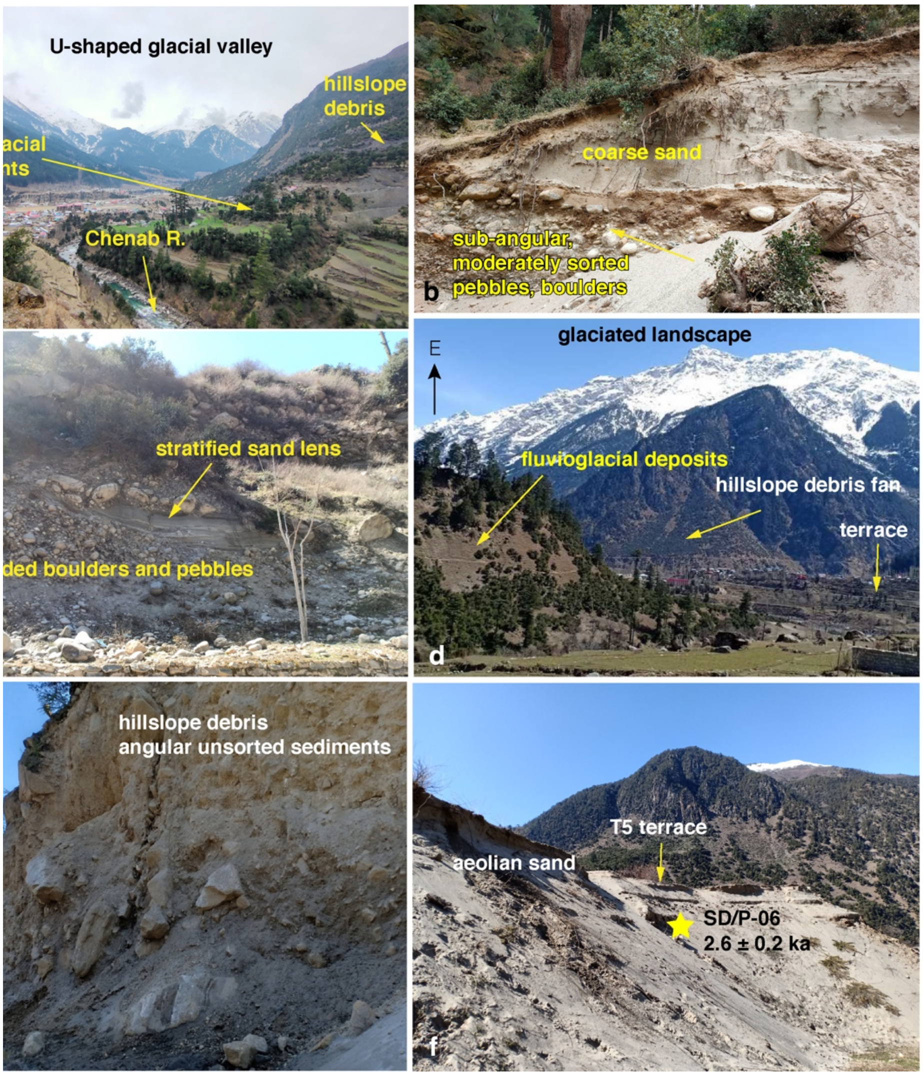


Figure 2: Field photographs. (a) U-shaped glacial valley in which Padder town is situated. Valley has subsequently been filled by fluvioglacial sediments and debris from the local hillslopes. (b) Fining upward section of fluvioglacial sediments in village Kundal. (c) Near the top of the sediment archive, well-rounded and well-polished pebbles and boulders suggest significant fluvial transport of sediments. (d) The steep valley walls of the Higher Himalaya often fail and generate cone or fan-shaped debris deposit. (e) The hillslope debris deposits are poorly sorted and disoriented. (f) Draping of aeolian fine- medium sand over the T6 terrace. Photograph taken while standing on the floodplain.

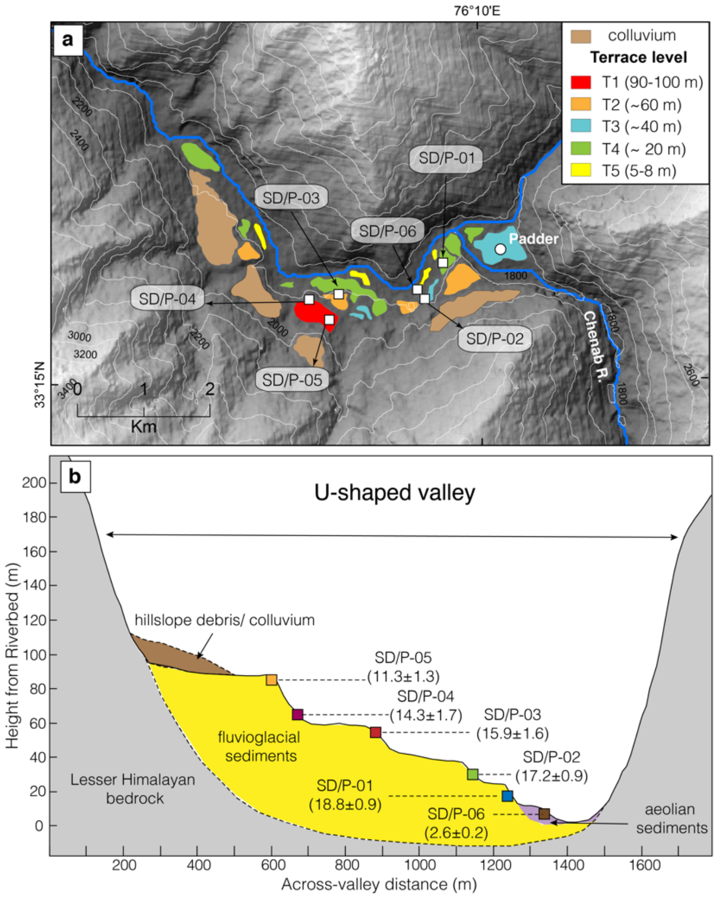


Figure 3: (a) Terrace map of the Padder valley showing at least five terrace levels above the present-day Riverbed. Locations of sample collection are shown. (b) A conceptual valley-profile drawn across the Padder valley showing aggradation during late Pleistocene and episodic re-incision of the aggraded valley-fills forming Holocene fill terraces.

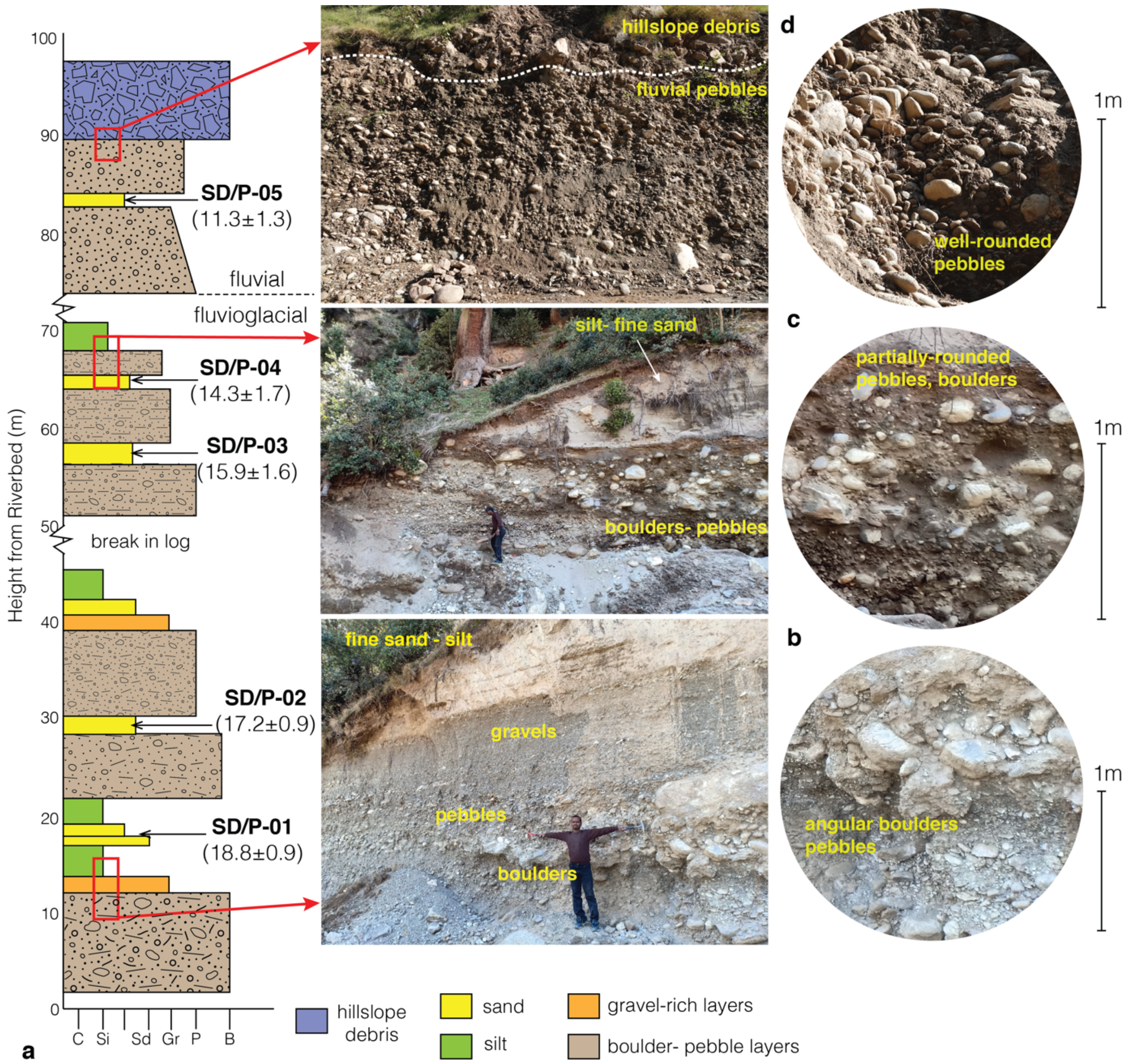


Figure 4: (a) Sediment-log and associated OSL ages from the sediment archive in Padder valley. Note that, the sediment record has breaks in between where proper exposures are not found (zagged line). (b) Poorly-sorted angular clast-dominated sediments at the base of the succession. Section shows an overall fining-upward sequence from boulders-pebbles to gravels to sandy silt. (c) Another fining upward sequence of fluvioglacial sediments from the middle of the litholog showing lesser angularity of the clasts. (d) Well-polished, well-rounded clasts from the top of the section suggesting long fluvial transport.

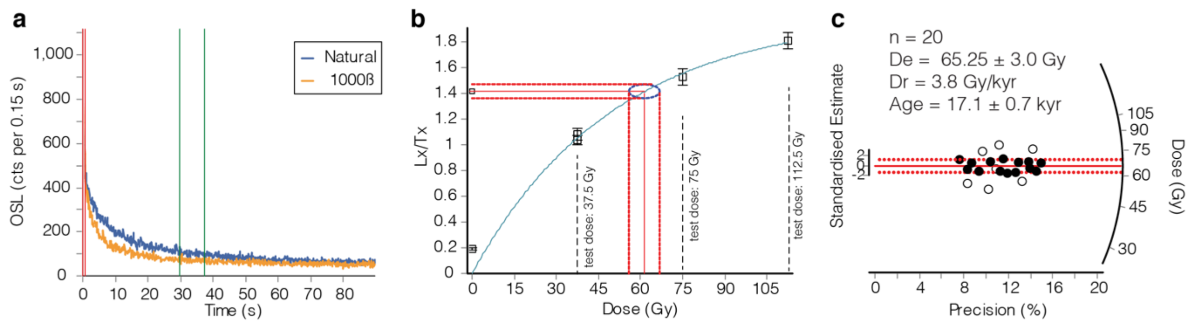


Figure 5: (a) Shine curve, (b) Dose growth curve and (c) Radial plot for De estimation for sample SD/P-02. Note that the black circles represent the aliquots used for the mean ± standard deviation estimation of De, while n represents the total number of aliquots that passed the filter criteria described in method section.

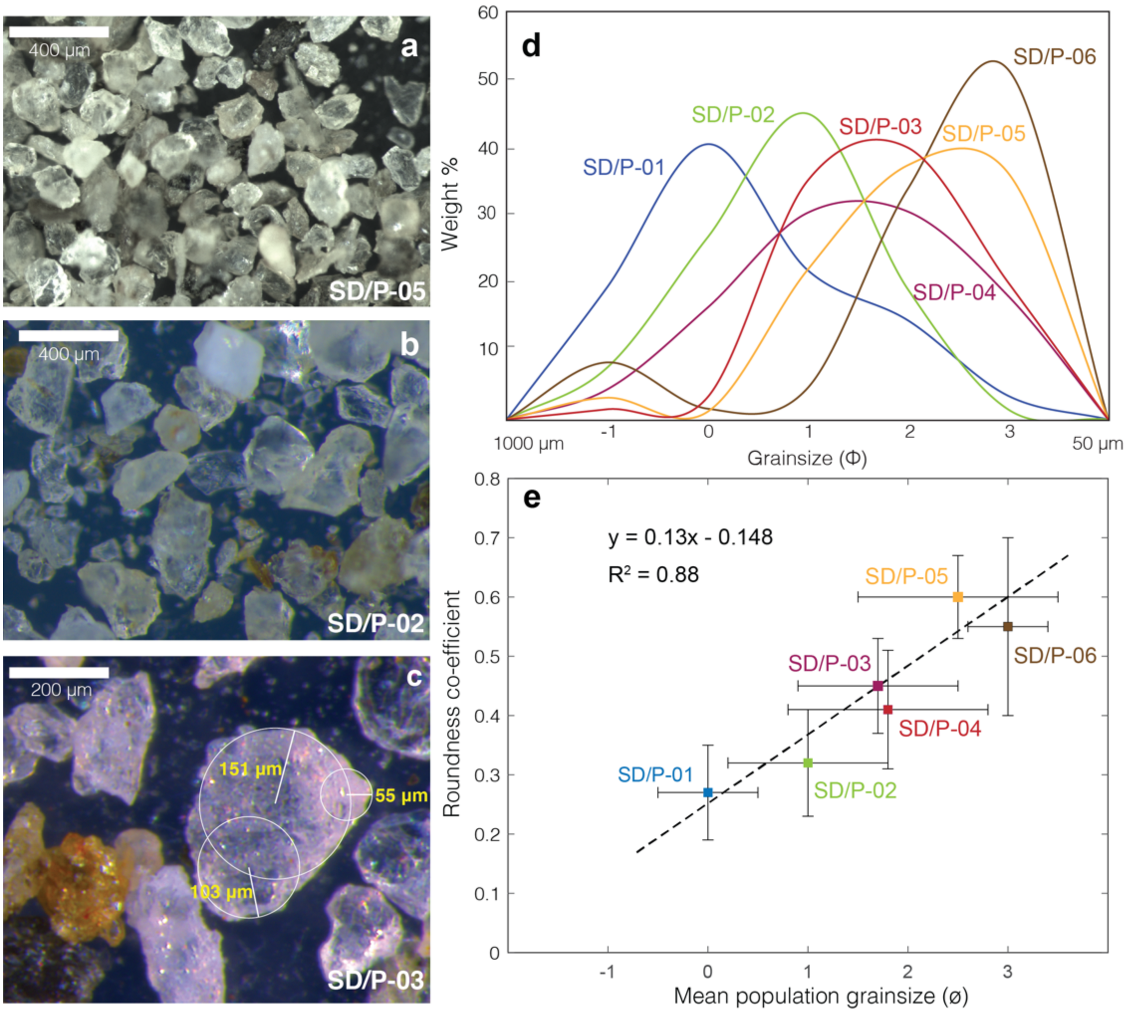

Figure 6: Photograph of sand samples (a) SD/P-05 and (b) SD/P-02 showing grainsize and grain-shape distribution. Note that, grains above 1000 µm and below 50 µm are discarded for easiness of measurement. (c) Photomicrograph of sample SD/P-03 showing how roundness co-efficient is measured by comparing the radii of the smallest and largest inscribed circle in single grains. (d) Grainsize distribution of sand samples. (e) Mean roundness co-efficient of quartz grains plotted against mean grain-size shows lowering of angularity and decrease of grain-size from the bottom to the top of the litholog, suggesting an increasing fluvial transport with time.

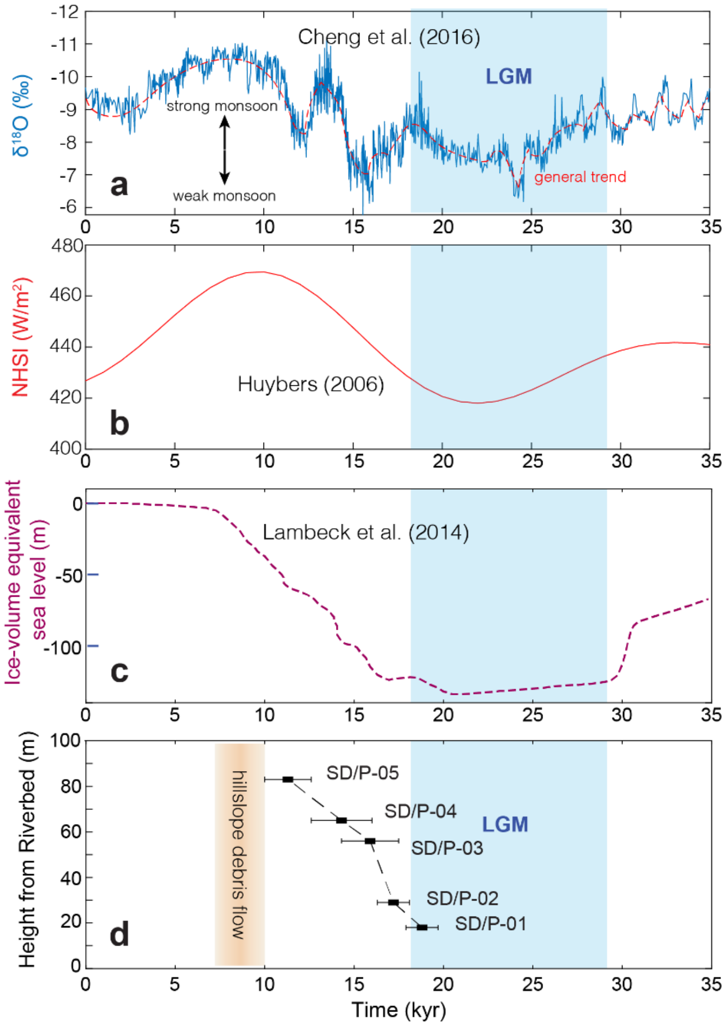


Figure 7: (a) Oxygen isotope ratio from Sanbao cave in China provides high-resolution data of climatic fluctuations and used for prediction of tele-connected changes in global climate (Cheng et al., 2016). (b) Northern Hemisphere Summer Solar Insolation (NHSI) at 30˚N

(Huybers, 2006) and (c) global sea-level curve (Lambeck et al., 2014). (d) Basin filling rate from Padder valley highlights the correlation of global temperature rise at glacial to interglacial phase transition leading to glacial melting and sediment aggradation in Padder valley.

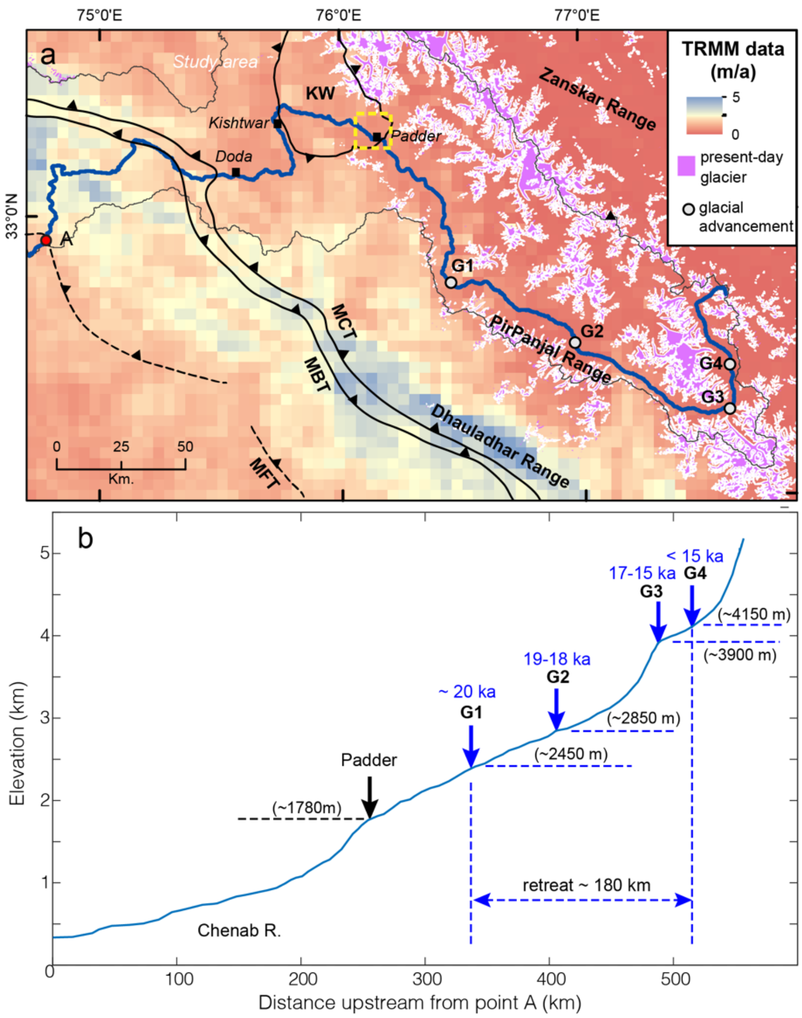


Figure 8: (a) Rainfall distribution map of the far-western Himalaya (TRMM data: Bookhagen and Burbank, 2006) and present-day glacial coverage map (GLIMS database) showing low present-day rainfall amount and proximity of the glaciated regions. (b) Longitudinal profile of the Chenab River showing past glaciated region and the location of Padder valley. Points G1-G4 mark the extent of glacial advancement during LGM (after Eugster et al., 2016). Note the rate of glacial retreat of ~180 km post-LGM during 20 – 15 ka.

Tables

| Sample | Latitude (˚) | Longitude (˚) | Height from river (m) | U (ppm) | Th (ppm) | K (%) | Moisture (%) | Dose rate (Gy/ky) | Paleo-dose (Gy) | OD (%) | Age (ky) |
|---|---|---|---|---|---|---|---|---|---|---|---|
| SD/P01 | 33.26515 | 76.16135 | 18 | 2.9 | 21 | 2.4 | 6 | 4.43±0.2 | 83±3 | 10.1 | 18.8±0.9 |
| SD/P02 | 33.26198 | 76.15896 | 29 | 3.3 | 13.8 | 2.1 | 8 | 3.78±0.1 | 65±3 | 11.6 | 17.2±0.9 |
| SD/P03 | 33.26187 | 76.13881 | 57 | 2.8 | 9.5 | 2.6 | 6 | 3.76±0.1 | 60±6 | 19.2 | 15.9±1.6 |
| SD/P04 | 33.26141 | 76.13258 | 65 | 3.5 | 12.9 | 2 | 6 | 3.5±0.1 | 50±6 | 20.4 | 14.3±1.7 |
| SD/P05 | 33.26035 | 76.13083 | 84 | 3.9 | 7.2 | 1.9 | 9 | 3.18±0.1 | 36±4 | 14.5 | 11.3±1.3 |
| SD/P06 | 33.26242 | 76.13725 | 4 | 3.3 | 15.5 | 2.5 | 10 | 4.26±0.1 | 11±1 | 6.2 | 2.6±0.2 |

Table 1: Sample location, elemental analysis and equivalent dose and depositional ages of sand samples (using OSL double-SAR protocol and central age model).